J Mater Sci (2020) 55:7652–7664

Composites & nanocomposites

The interaction between *N*,*N*-dimethylacrylamide and pristine graphene and its role in fabricating a strong nanocomposite hydrogel

Ailin Gao[1], Shuju Chen[1], Shuai Zhao[1], Guangfa Zhang[1], Jian Cui[1], and Yehai Yan[1,*]

[1] Key Lab of Rubber-Plastics, Ministry of Education/Shandong Provincial Key Lab of Rubber-Plastics, School of Polymer Science and Engineering, Qingdao University of Science and Technology, Qingdao 266042, China

Received: 30 August 2019
Accepted: 6 March 2020
Published online: 19 March 2020

ABSTRACT

In this work, mechanically strong and electrically conductive poly(*N*,*N*-dimethylacrylamide) (PDMAA)/pristine graphene (GR) nanocomposite hydrogel was synthesized by directly dispersing pristine GR into *N*,*N*-dimethylacrylamide (DMAA) monomers, which have been commonly used to prepare polymeric hydrogel as reactive monomers. Results showed that the introduction of GR nanosheets as physical cross-linking and its cooperation with organic cross-linker *N*,*N*-methylene bisacrylamide (BIS) were found to efficiently improve the mechanical strength, dimensional homogeneity of pore structure, thermal and electrical conductivity of resultant PDMAA hydrogels. More importantly, the intrinsic interaction between DMAA monomer and GR was systematically analyzed by ultraviolet–visible (UV–Vis) spectrophotometer, nuclear magnetic resonance (^{1}H NMR) and rheological test for the first time. These studies help us understand the formation mechanism of PDMAA hydrogel when graphene was added, as well as the fundamental parameters that govern the properties of hydrogels.

Introduction

Most polymeric hydrogels lack sufficient mechanical strength and functionality, especially the electrical and thermal conductivity [1–3]. To overcome the above limitations, organic/inorganic additives were broadly introduced into polymer base to construct composites [4–8]. In the composites, the nanomaterials have substantially larger surface area than micro-sized fillers, offering a higher degree of interaction at the molecular scale against polymer chains [9]. Very small amount of nanomaterials can efficiently improve many properties without compromising other desirable properties, expanding the application fields of hydrogels to biomedicine, environmental protection and sensors, etc. [4, 10–12]. In addition, the introduction of nanoscale fillers can also solve problems such as poor optical transparency, low water

Address correspondence to E-mail: yhyan@qust.edu.cn

https://doi.org/10.1007/s10853-020-04542-5

absorption and brittleness caused by merely employing traditional chemical cross-linking agents [13]. So far, various nanofillers have been developed involving TiO_2, hydrotalcite, clay, carbon nanotubes and graphene, etc., to create various functional hydrogels [14–17]. The dispersion mode of nanomaterials into hydrogels is generally divided into three ways: [9] direct immobilization on hydrogel, non-covalent combination such as intermolecular forces and covalent combination. The uniform and stable dispersion of nanomaterials in hydrogel has a great influence on their mechanical properties, electrical conductivity and thermal conductivity.

Specially, graphene-based carbon nanomaterials have been intensively studied as a type of nanofiller owing to its large surface area ($\sim$ 2630 m^2/g), flat structure, as well as its intrinsically excellent optical, thermal, electrical and mechanical properties [11, 18]. In order to successfully link to the polymer chains, graphene was mainly modified by chemical or physical methods to endow its surface with functional groups and the ability to interact with initiator or monomers [19]. When the coupling termination occurred during the reaction process, the graphene connected to the end of polymer chains could play the role of cross-linking points and help to form a polymer network.

Graphene oxide (GO) is the mostly used graphene-based nanofiller due to its good dispersion capacity in water [11, 20–22], which is the essential factor to construct hydrogels. Its hydrophilic surface caused by lots of active functional groups such as –OH and –COOH also made GO readily interact with monomers and initiators. Incorporation of GO was a feasible way to synthesize functional composite hydrogel, involving thermo-sensitive, gas-sensitive and adsorptive characteristics [23]. However, GO is limited by no or low conductivity and much reduced strength due to the loss of electrical conjugation of contiguous aromatic carbon lattice during the oxidation process. To obtain electrical conductive polymeric hydrogel, GO should be further reduced by various chemical or thermal treatments, which required polymers great chemical stability or thermal stability. Low-oxidation graphene has also been developed as substitution, which was certainly solution-processable and electrical conductivity [24]. Yet the remained functional groups still seriously destroyed the crystal structure of graphene, and obvious improvement of electrical and thermal conductivity was still hard to realize. A few works about synthesizing polymer/pristine GR hybrid hydrogel have been reported, for the reason that the dispersion of unmodified pristine GR sheets in water has usually been considered unattainable. Special dispersants or fabricating strategy was thus necessary to break that deadlock. For instance, Liu successfully synthesize epoxy/pristine GR hydrogel, wherein alkali lignin was used to inhibit the aggregation of GR sheets in aqueous solution [25]. Hou et al. fabricated pristine GR–polymer hydrogel by immersing the primary three-dimensional GR hydrogel into polymer monomer solution and initiating the in situ free-radical polymerization of monomers [26].

Owing to the intrinsic hydrophilic, chromatic, great adhesiveness and biocompatible properties, hydrogels based on PDMAA have found numerous applications in life science and medical treatment, such as intervertebral disk prosthesis, drug-release stents, contact lenses and cardiac valves [27–29]. In addition, the double bonds and amide groups endow DMAA monomers with reactive sites to generate various functional hydrogels. For example, self-healing, thermal-sensitive or high blood compatibility PDMAA-based hydrogels could be obtained by grafting or copolymerization approach [30–32]. However, its low mechanical strength in the chemically cross-linked gel is still a dominate limitation to prevent its practical use.

This work aims to directly create PDMAA/pristine GR nanocomposite hydrogel with outstanding mechanical and conductive performance without extra reducing treatments or auxiliary dispersant. Strong interaction between DMAA and pristine GR is the key factor for allowing the dispersion of pristine GR into DMAA monomers, which was certified in this work. Several detecting means like UV–visible spectrophotometer, ^1H NMR and rheological test were applied to understand the interaction mechanism between GR nanosheets and DMAA. The mechanical, swelling and conductivity measurements were also investigated in detail.

Materials and experiments

Materials

N,*N*-dimethylacrylamide (DMAA) was purchased from Chengdu Best Reagent Co., Ltd (China). *N*,*N*-methylene bisacrylamide (BIS, purity 99%) was purchased from Aladdin Chemical Co., Ltd. Natural graphite (purity > 99%, 300 mesh) was brought from Qingdao Haida Co., Ltd (China). *N*,*N*-dimethylformamide (DMF) and pyridine (purity > 99.5%) were purchased from Tianjin Fuyu Fine Chemical Co., Ltd (China). Hexane with purity of 98%, ethyl alcohol with purity of 99.7% and hydrochloric acid (HCl) with purity of 37% were purchased from Laiyang Fine Chemical Plant Co., Ltd (China). Ammonium persulfate (APS, purity 98%) was purchased from the Tianjin Baxsn Chemical Co., Ltd (China). Tetramethylethylenediamine (TEMED, purity 99.5%) was supplied by Shanghai Zhanyun Chemical Co., Ltd (China). Ultrapure water (18.25 MΩ) was produced in the laboratory using ULUPURE (UPLHeI-20T).

Fabrication of DMAA/GR composite suspension

GR was synthesized via classical potassium intercalation and liquid phase stripping method. The obtained GR solid was successively washed with acid, water and DMF to remove the impurities in the product. A homogeneous GR/DMF suspension was yield after multiple steps involving mechanical stirring, static settlement, taking supernatant and redispersing. Finally, a certain volume of GR/DMF dispersion with known concentration was washed with DMAA to replace DMF with DMAA. Thus, the required concentration of DMAA/GR dispersion was prepared.

Fabrication of PDMAA/GR nanocomposite hydrogel

Take the preparation of PDMAA/GR hydrogel with 0.4 wt% GR as an example: (1) Firstly, 0.5 mL DMAA/GR dispersion was added into a reaction flask and performed ultrasonic treatment for 30 min under ice-water bath. (2) 1 mL BIS aqueous solution with a concentration of 0.962 mg/mL and 0.9 mL TEMED aqueous solution with a concentration of 1.54 μL/mL were dropped into the above dispersion with shaking the flask gently to prevent local overheating and letting set for 10 min. (3) Nitrogen was flowed into the reaction flask for 10 min, and the flask was subsequently moved into ice-water bath to ultrasound for 10 min. (4) 0.1 mL APS aqueous solution with a concentration of 24 mg/mL was slowly injected into DMAA/graphene dispersion with shaking the bottle gently and ultrasound for 5 min. (5) The mixture was placed into ice-bath for 30 min and transferred into oil bath under 35 °C for 24 h. The polymerization proceeded slowly.

By changing the content of GR against DMAA, PDMAA/GR hydrogels with mass fraction of 0–1.5% were prepared. The mass fraction of GR was calculated based on the mass difference between the dry hydrogel and DMAA monomers. The code and corresponding composition of various PDMAA/GR hydrogels are shown in Table 1.

Characterizations

UV–Vis (TU-1901PC) was used to characterize the interaction between DMAA monomers and GR nanosheets, wherein the diluted DMAA/water solution and DMAA/GR/water suspension (60 μL/mL) were, respectively, scanned between 900 and 190 nm. Before that, the pure water was scanned between the same wavelength range to deduct background adsorption. The total reflectance Fourier-transform infrared spectrums (ATR-FTIR) were detected by a Bruker VERTEX 70 spectroscopy. ^{1}H NMR (Bruker AVANCE III 500 MHz) profiles of DMAA in D_2O and DMAA/GR suspension in D_2O were also determined to further verify the interaction between DMAA monomers and graphene sheets. To obtain DMAA/GR/D_2O suspension, centrifugation (10000 r/min × 20 min) was performed to the original DMAA/GR suspension and the precipitation in bottom layer was taken out to being redistributed in D_2O by the aid of ultrasonic treatment. Morphologies of hydrogels were measured via scanning electron microscopy (SEM, JEOL JSM-7500F), wherein both the skin and cross section were viewed. Before the SEM observation, the hydrogel samples for SEM were first cooled in liquid nitrogen for 15 min and then dried in a freeze dryer for 12 h to thoroughly remove water.

Tensile properties and compression performance of as-prepared hydrogels were tested by universal material testing machine (Zwick/Roell Z005). The

Table 1 Compositions of PDMAA/GR hydrogels and their responding codes

Hydrogel	Compositions				Water/wt%
	DMAA/mg	BIS/wt%	GR/wt%	APS/wt%	
PH	481	0	0	0.5	80.6
PBH	481	0.4	0	0.5	80.6
$PG_{0.4}H$	481	0	0.4	0.5	80.6
$PG_{0.7}H$	481	0	0.7	0.5	80.6
$PBG_{0.1}H$	481	0.4	0.1	0.5	80.6
$PBG_{0.4}H$	481	0.4	0.4	0.5	80.6
$PBG_{0.7}H$	481	0.4	0.7	0.5	80.6
$PBG_{1.0}H$	481	0.4	1.0	0.5	80.6
$PBG_{1.5}H$	481	0.4	1.5	0.5	80.6

"wt%" of BIS, GR, APS and water all indicate their mass ratio against DMAA monomers

testing was carried out at ambient temperature with preloading force of 0.05 N, preloading speed of 50 mm/min, tensile speed of 30 mm/min and clamp spacing of 60 mm. The compression performance was tested with preloading force of 0.2 N, preloading speed of 15 mm/min, compression speed of 10 mm/min and clamp spacing of 25 mm.

To further investigate the effect of GR nanosheets on the mechanical strength of PDMAA hydrogel, an ARES-G2 rheometer was used with a plate-plate sensor (25 mm diameter, gap of 1.5 mm). Both strain scanning and frequency scanning modes were involved to determine the dependency of storage modulus (G') and loss modulus (G'') on GR contents. For the strain scanning mode, the strain range was 0.01–100% with a fixed frequency value of 6.28 rad/s. For the frequency scanning mode, the frequency range was varied from 100 to 0.04 rad/s with a fixed strain of 1%.

Cylindrical hydrogels with diameter of 13 mm and height of 10 mm were used for swelling property test. Their original weight was represented as W_0. The swelling test was carried out via soaking these dry samples in ultrapure water and weighing them at intervals, until reaching to the swelling equilibrium. The samples' weight at different soaking time was remarked as W_t. Before weighing, the water on the hydrogel surface was wiped gently with filter water. The swelling ratio for different soaking time was calculated based on the equation $q = \frac{W_t}{W_0}$. The porosity of hydrogel samples was calculated based on the following formula: [33]

$$P = \left(1 - \frac{\rho}{\rho_0}\right) \times 100\%$$

wherein ρ is the apparent density and ρ_0 is the bulk density of hydrogel. The bulk density was directly detected by a densitometer (AU300S, Hangzhou Jinmai instrument Co., Ltd). To measure the apparent density, the volume and weight of prepared hydrogel were measured.

The conductivity including thermal conductivity and electrical conductivity was measured. The thermal conductivity was determined by a DTC-300 thermal conductivity instrument, while the electrical conductivity was determined using a four-probe PC68 high resistance meter.

Results and discussion

In the current work, pristine GR was directly used as nanofillers to synthesize mechanically strong and electrically conductive polymer-based nanocomposite hydrogel. It was found in our work that pristine GR could readily disperse in DMAA monomers, which made it possible to directly fabricate conductive PDMAA/GR hydrogel via applying DMAA acting as both reactive monomers and dispersing

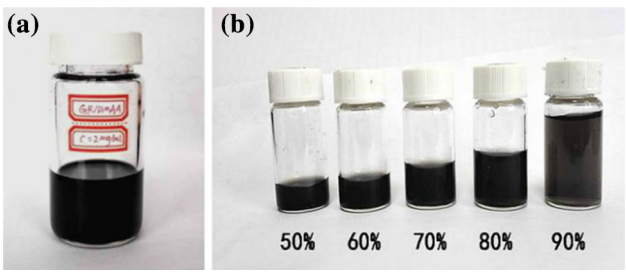

Figure 1 **a** DMAA/GR dispersion. **b** Different water contents of DMAA/GR/water mixture dispersion after standing for 12 h.

solvent. The digital image as shown in Fig. 1a is the DMAA/GR suspension, which could still keep its stable homogeneous state after two days of stationary. No sedimentary particles could be found. Water is commonly needed as solvent in the hydrogel system, and higher water content can achieve higher porosity. However, the introduction of water into DMAA/GR suspension may break the homogeneous state because of the poor dispersibility of hydrophobic GR in water. Thus, we prepared DMAA/GR/water dispersions with different water contents from 50 to 90% to determine the highest amount of water that could be added. As shown in Fig. 1b, there was no deposition at the bottom of the mixture suspension with water content below 80% after standing for 12 h; inversely, obvious deposition could be observed with water content over 90%. Therefore, a water mass ratio of 80% was preferred in the following procedure. The morphologies and quality of prepared GR nanosheets could be found in our previously published research [34].

The excellent dispersibility of pristine GR in DMAA originates from the strong interaction between DMAA molecule and GR nanosheets. DMAA is a kind of acrylamide monomers which structure formula is CH_2=CHCON$(CH_3)_2$. The hydrogen atoms on amide nitrogen are substituted by methyl group. And driven by two methyl groups connected with nitrogen atom, a hyper-conjugated system involving nitrogen, carbonyl and double bond is formed between nitrogen, which will theoretically supply π–π interaction with the GR nanosheets [35]. To verify the existence of such interaction between DMAA and GR nanosheets, UV–Vis adsorption profiles and ^{1}H NMR profiles of DMAA/water and DMAA/GR/water solution were researched. As shown in Fig. 2a, the single DMAA/water solution showed adsorption peaks at 198 nm and 233 nm, which belong to the –C=C–C=O (π–π transition) and –N$(CH_3)_2$ (n–π transition) structure in DMAA, respectively. When graphene was added, the position of absorption peak for π–π transition obviously changed to 205 nm and that for n–π transition changed to 234 nm, as shown in Fig. 2b. It was speculated that the adsorption force of graphene to DMAA molecule resulted in the decrease in electron cloud density and the red shift of UV–Vis absorption spectrums. The ATR-FTIR spectrums of solid pure PDMAA hydrogel and PDMAA/GR hybrid hydrogel are displayed in the revised Fig. 2. Slight red shift is observed in Fig. 2c for the C=O position, from 1617 cm^{-1} for pure PDMAA hydrogel to 1619 cm^{-1} for PDMAA/GR hybrid hydrogel. Such results further validate the decreased electron cloud density of C=O groups caused by the conjugation effect between C=O and GR nanosheets.

^{1}H NMR spectrums are depicted in Fig. 3. The chemical shifts of main signal peaks in Fig. 3a were as follows: 6.56 (a), 5.97 (b), 5.62 (c), 2.95 (d) and 2.81 (e), corresponding to the theoretical chemical shift of protons in the molecular structure of pure DMAA. In comparison, the chemical shifts of DMAA/GR in Fig. 3b showed obvious red shift phenomenon, proving the truly existence of interaction between GR and DMAA. Considering that there was no hydrogen atom on the amide groups in DMAA molecule, the role of hydrogen bonds could be eliminated [36]. The phenomenon that the chemical shift of DMAA moved to low field with the existence of GR demonstrated the decrease in the electron cloud density of each H in DMAA molecule, indicating the effect of electron absorption from GR nanosheet. These above results were consistent with the analysis results of ultraviolet testing, further confirming the strong interaction between DMAA and pristine GR.

The strong interaction between DMAA and GR can play the role as physical cross-linking points, but organic cross-linker such as BIS was still needed to supply more and stronger cross-linking points. Therefore, three kinds of hydrogels, marked as PH (pure PDMAA), PGH (PDMAA/GR hydrogel without BIS) and PBGH (PDMAA/GR hydrogel with BIS), were prepared, respectively. Without adding GR and BIS, pure PDMAA hydrogel has poor formability, weak mechanical strength and compression recovery, which made it difficult to continue its quantitative testing and practical usage. The addition of GR endowed PGH hydrogel with improved formability and compress recovery, wherein most of the deformation could be restored (as observed in Fig. 4b). The uniform color and morphology without agglomerated particles indicated the excellent dispersion of GR in PDMAA matrix. In contrast, PBGH sample showed the best formability and mechanical strength including better stretching, compression and loading performance. As showed in the digital photographs summarized in Fig. 4c1–c3, no matter under stretching or compression, the hydrogel could completely recover from its initial length or height after release, showing great

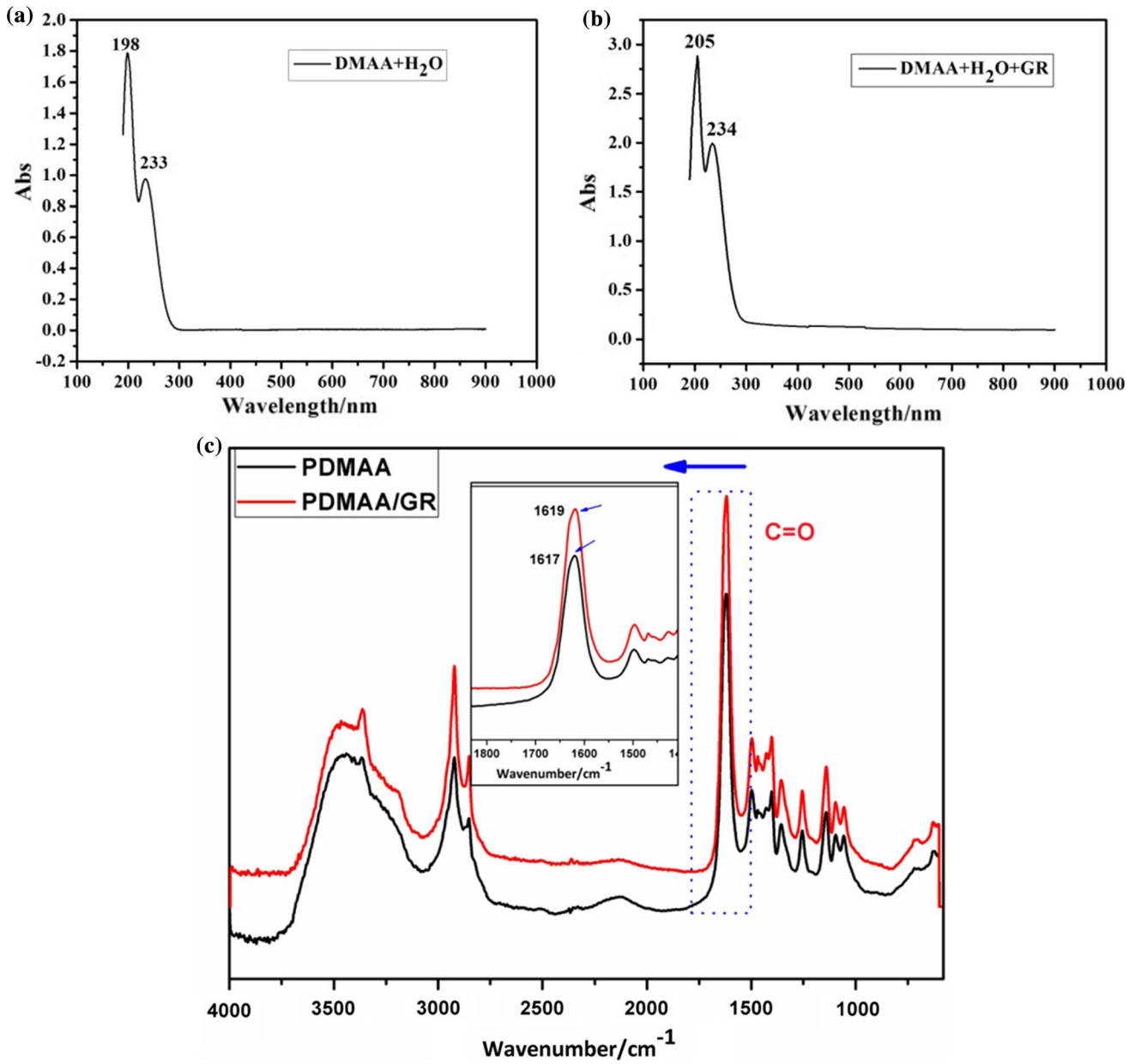

Figure 2 UV–Vis absorption spectrums of **a** DMAA in water and **b** graphene/DMAA aqueous dispersion. **c** ATR-FTIR spectrums of pure PDMAA hydrogel and PDMAA/GR nanocomposite hydrogel.

resilience. And it could withstand certain load up to 10 g. It could be concluded that GR improved the formability and mechanical properties to a certain degree, while organic cross-linker was necessary to constitute robust hydrogel.

The SEM images of PBH and PBGH are depicted in Fig. 5 to explain the effect of GR nanosheets on the pore structure of PDMAA hydrogel. For PBH sample merely using BIS as cross-linker, it has uneven pore size with large pores at a size of several micrometers and small pores below 100 nm, demonstrating the usually random cross-linking phenomenon caused by chemical cross-linkers [37]. Such uneven pore structures and thin walls may weaken the mechanical properties of resultant hydrogel. The pore structures of PBGH with the coordination of graphene and BIS were significantly different from the control one. Relatively, regular pores with similar size (about 5 μm) and much thicker walls are observed in Fig. 5c, d. Accordingly, the well-dispersed graphene nanosheets could not only act as physical cross-linking points but also regular the internal cross-linking

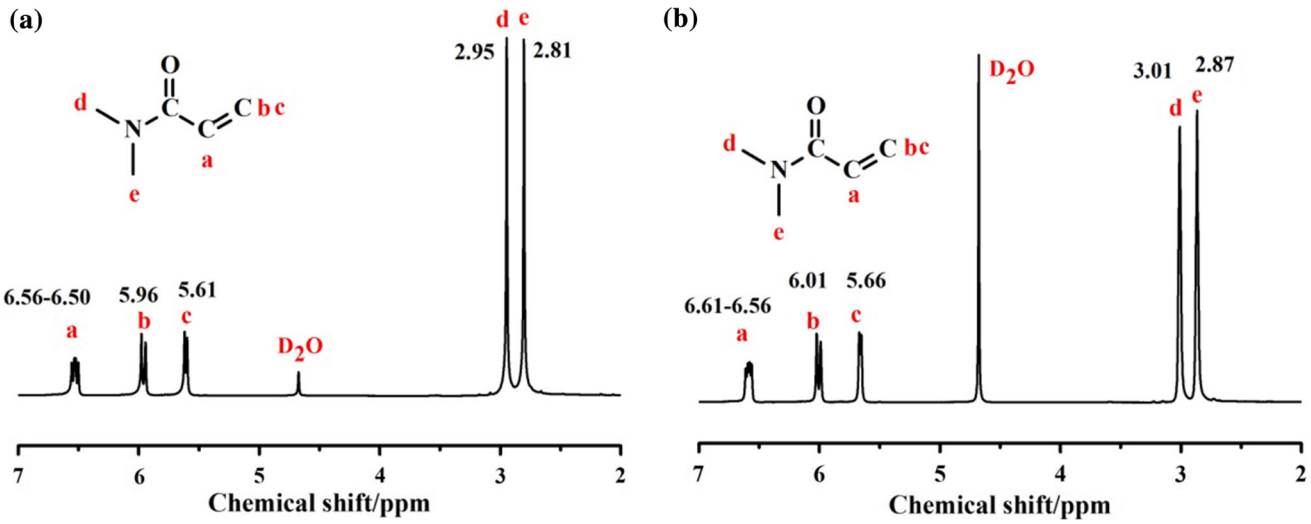

Figure 3 ^{1}H NMR spectrums of **a** DMAA in D_2O and **b** graphene/DMAA in D_2O.

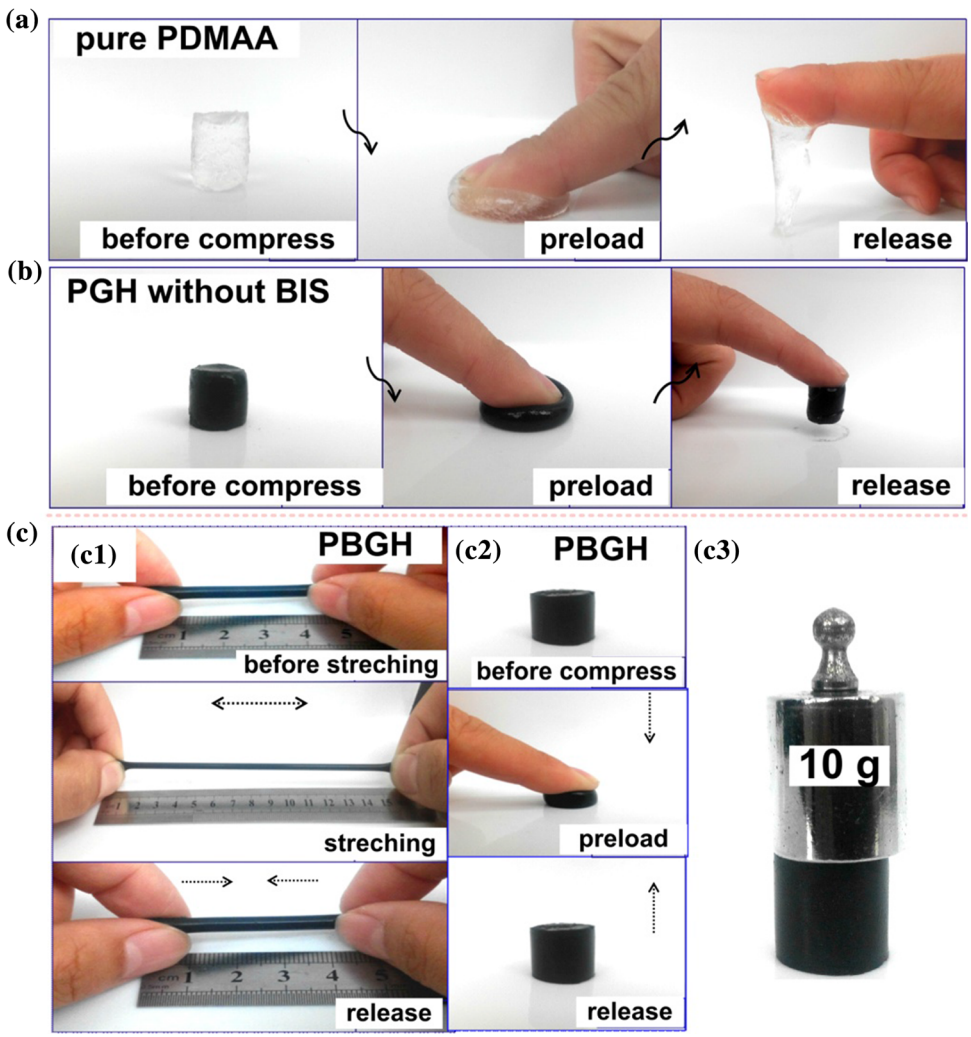

Figure 4 Macroscopic tensile and compressive performance test of PDMAA-based hydrogel: **a** PH, **b** PGH (GR 0.4%), **c** PBGH (BIS 0.4% and GR 0.4%).

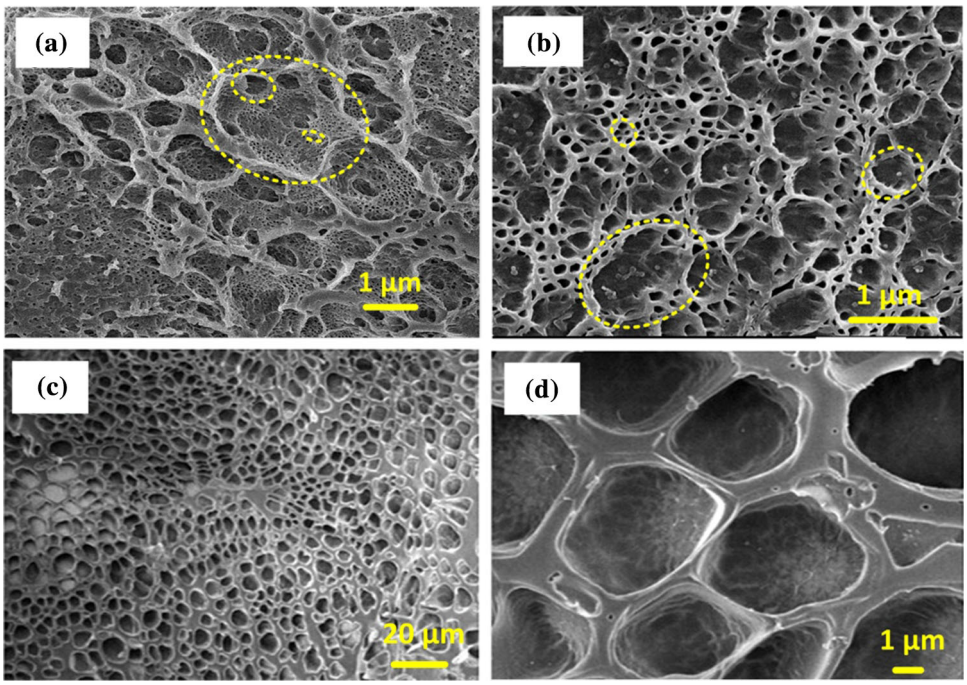

Figure 5 SEM views of **a** the surface of PBH (without GR); **b** the cross section of PBH; **c** the surface of PBGH (with GR); and the cross section of PBGH.

structure of hydrogel. The porosity of PBH and PBGH samples was 91.4% and 94.5%, indicating a higher porosity of PDMAA/GR composite hydrogel.

To further investigate the effect of GR nanosheets on the mechanical properties, a series of PDMAA/GR nanocomposite hydrogels with various GR contents from 0 to 1.5% were synthesized. The tensile and compression performance of all samples is summarized in Fig. 6 and Table 2. The tensile stress–strain curves of hydrogels showed that with GR content below 1.0%, the tensile strength increased gradually with the increase in GR content from 51.5 kPa for 0% to 96.6 kPa for 1.0%, while decreased to 62.6 kPa when the graphene content was 1.5%. The elongation at break experienced the similar varying tendency with first increase from 156% for 0% to 246% for 1.0% and succedent decrease to 193%. A small quantity of GR played a reinforcing role owing to its dual functions of cross-linker and nanofillers. For our PDMAA/GR nanocomposites, the obvious reinforcement of PDMAA hydrogel by GR is attributed to the homogeneously dispersion of GR nanosheets throughout the PDMAA matrix and their strong interfacial interaction. The existed interaction

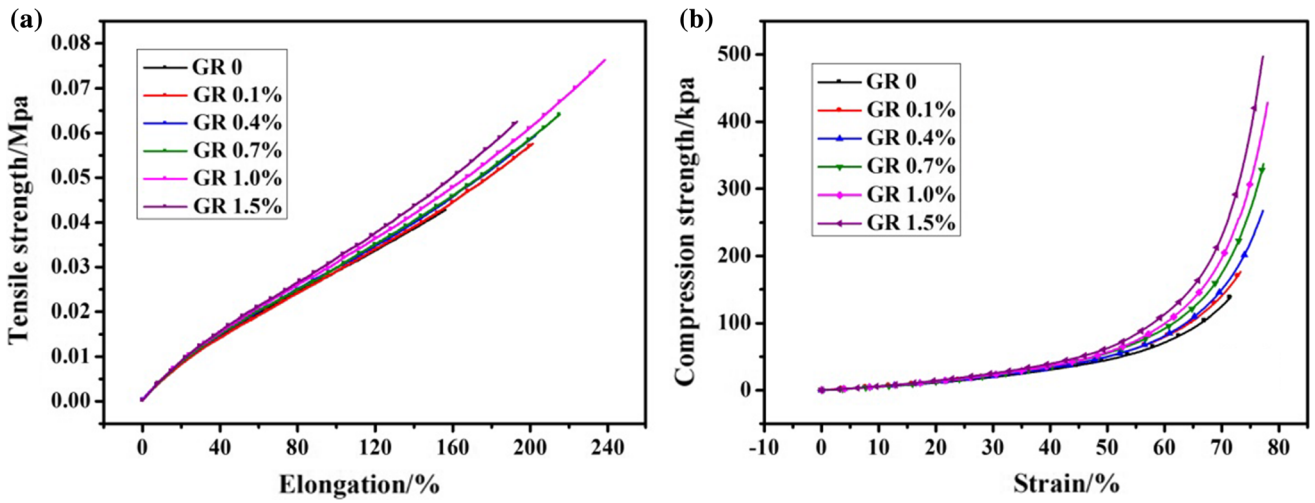

Figure 6 Tensile stress–strain and compression stress–strain curves of PDMAA/GR nanocomposite hydrogels.

Table 2 Mechanical properties of PDMAA/graphene nanocomposite hydrogels

Sample	Tensile test			Compression test		
	Modulus/kPa	Strength/kPa	Elongation at break/%	Modulus/kPa	Strength/kPa	Fracture strain/%
PBG_0H	23.8 ± 0.1	51.5 ± 1.5	156 ± 3.7	112.4 ± 3.9	201 ± 10.5	70.6 ± 0.5
$PBG_{0.1}H$	24.6 ± 0.4	60.2 ± 1.3	193 ± 2.9	121.1 ± 2.2	237 ± 1.0	72.5 ± 0.5
$PBG_{0.4}H$	25.0 ± 0.3	63.0 ± 2.1	212 ± 7.4	129.2 ± 2.5	295 ± 35.5	76.5 ± 0.5
$PBG_{0.7}H$	25.5 ± 0.1	68.3 ± 4.0	223 ± 7.5	137.4 ± 2.7	366 ± 14.5	78 ± 0.7
$PBG_{1.0}H$	26.4 ± 0.1	96.6 ± 4.5	246 ± 16.8	142.6 ± 2.1	421 ± 7.1	80 ± 0.3
$PBG_{1.5}H$	27.8 ± 0.2	62.6 ± 1.4	193 ± 15.6	172.9 ± 2.2	497 ± 13.7	78.7 ± 1.3

between PDMAA and pristine GR leaded to the stress transfer effect. When the hydrogel was subjected to external forces, partial forces could be rapidly transferred from polymer chains to adjacent GR nanolayers, evenly distributing the external force and increasing tensile strength. In addition, as rigid particles the GR nanosheets could be assumed as local heterogeneity and cause stress concentration, avoiding the destruction of polymer matrix [38]. GR can not only induce crazing and shear band, but also terminate the development of craze and shear band into destructive crack.

Figure 6b shows the compressive stress–strain curves of PDMAA/GR hydrogels with GR mass fraction from 0% to 1.5%, respectively. It can be seen that both compressive strength and fracture strain continuously increased with the increase in GR content. The reason is that the addition of GR has decreased the density of chemical cross-linking points and the length of the chain segments between cross-linking points was larger, originating from the strong physical interaction between GR and polymer which competed with chemical cross-linking. When subjected to external force, polymer chain segments had relatively higher movement ability and could be adjusted to the force direction in time. The addition of GR gave the hydrogel a certain mechanical strength and loading capacity during compression, which induced matrix yield and flexible response to compression. More importantly, the regular pore structure and thicker walls as shown in SEM views were also helpful for enhancing the compressive strength and deformation.

To deeply understanding the effect of GR on the mechanical properties of hydrogel and the interaction between GR and polymer, rheological measurements involving frequency scanning and strain scanning were investigated. Firstly, the storage modulus–frequency curves of PBGH samples with various GR contents from 0% to 1.0% are depicted in Fig. 7a. All curves experienced two obvious decreases versus the increase in frequency: one at 0.1 Hz and the other at 90 Hz, implying the destruction of internal structure of hydrogel in those two positions. At low frequencies (below 0.1 Hz), the storage modulus of all samples remained stable owing to the sufficient movement of polymer chains. As frequency over 0.1 Hz, the decoupling speed of polymer chains was faster than the re-entanglement speed, leading to the obvious decrease in storage modulus. With the further increase in frequency, polymer chains began to orient and decompose along the direction of external force, which showed a stable storage modulus at macro-level. Finally, with frequency over 90 Hz, the movement of polymer chains cannot keep up with external force and segments freezing phenomenon occurred. In addition, the chemical bonds might break, leading to a sharp decline in the storage modulus. Considering the difference of curves between various GR contents, conclusion could be made that higher amount of GR positively improved the storage modulus of hydrogel. Compared with the curve corresponding to 0% GR, the other four curves showed a more significant decrease at the frequency around 0.1 Hz, for the reason that GR nanosheets hindered the chain movement. The destruction of physical cross-linking between GR and polymer mainly occurred at this stage.

Strain scanning was performed to PH and $PG_{0.7}H$ to deeply investigate the effect of GR on the rheological properties of PDMAA hydrogel without the interference of BIS. From Fig. 7b, it can be seen that the G' of both PH and $PG_{0.7}H$ was always higher than the corresponding G'', indicating that the rheological

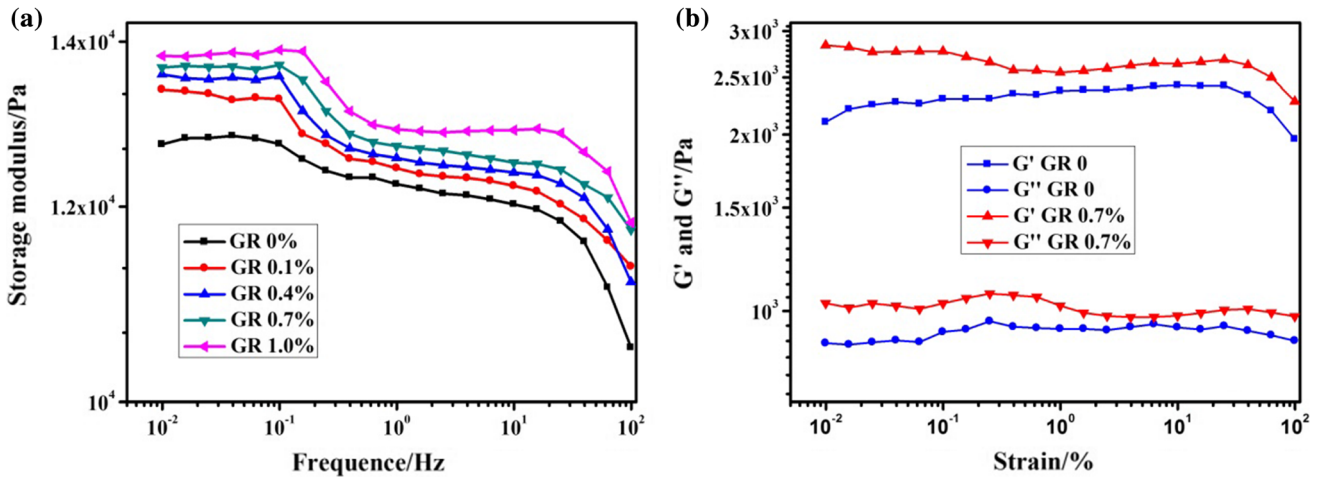

Figure 7 Rheology scanning test of PDMAA/GR nanocomposite hydrogel: **a** storage modulus–frequency changes from 0.01 to 100 Hz of PBGH hydrogels with various graphene contents; **b** the change of G' and G'' versus strain from 0.01 to 100% of PGH hydrogels without adding BIS.

behavior of both hydrogels was closer to a solid. However, G' and G'' values of $PG_{0.7}H$ were always higher than those of PH. The higher G' value of $PG_{0.7}H$ could be attributed to its higher cross-linking degree caused by the excellent interactions between GR and PDMAA. The higher G'' of $PG_{0.7}H$ could also be attributed to the interaction between GR and PDMAA, which would hinder the movement of polymer chains, increase friction force and cause strain to lag behind stress. However, the interaction was unstable and readily destroyed by external force. Therefore, with the increase in strain, slightly decline of G' and G'' of $PG_{0.7}H$ was observed (0.1–1% of strain for G' and 1–10% for G''). The destruction and reconstruction of interaction between GR and PDMAA coexisted, which can explain why the G' and G'' were always higher than that of PH under the whole strain range. The rheological measurement results demonstrated the reinforcement effect of GR on the mechanical properties of PDMAA hydrogels.

The swelling properties of hydrogels (PBH, $PBG_{0.1}H$, $PBG_{0.4}H$, $PBG_{0.7}H$ and $PBG_{1.0}H$) were determined, and the information of swelling ratio and swelling rate versus swelling time is depicted in Fig. 8. For all samples, their swelling rates and swelling ratios uniformly and rapidly grew within 25 min. With the extension of swelling time, the swelling ratio increased slowly and tended to be stable, indicating the reaching of swelling equilibrium. In the later stage, the growing rates of swelling ratio of hydrogels with GR as additives were always higher than the control one and positive correlation

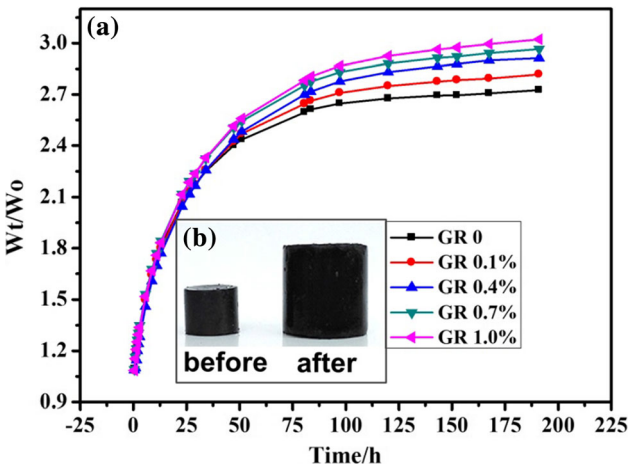

Figure 8 Swelling properties of PDMAA/GR nanocomposite hydrogels.

was found between swelling ratio and GR contents. The highest swelling ratio of about 3.1 belonged to $PBG_{1.0}H$, which was much higher than 2.7 corresponding to PBH. When the stretching force caused by water diffusion is larger, the hydrogel shows the swelling phenomenon in volume. The dispersion of GR in PDMAA hydrogels leaded to the formation of more micro-cracks, which can increase the amount of micropore structures, weaken the hydrogen-bond interaction between polymer chains, help the water molecule diffuse into hydrogel system and hence bring out larger swelling ratio.

Due to the direct addition of pristine GR into PDMAA hydrogel, it was supposed that the conductivity should be improved without any reduced

Table 3 Thermal conductivity of PDMAA/GR nanocomposite hydrogels

Sample	Thermal conductivity (W/m K)		The increment of thermal conductivity (W/m K)	
	1#	2#	1#	2#
PBH	0.466	0.470	–	–
$PBG_{0.1}H$	0.483	0.484	0.017	0.014
$PBG_{0.4}H$	0.498	0.505	0.032	0.035
$PBG_{0.7}H$	0.521	0.527	0.055	0.057
$PBG_{1.0}H$	0.536	0.543	0.070	0.073

treatment. Table 3 shows the thermal conductivity changed with the increment of GR mass fraction. It increased to near 0.54 W/(m K) when the GR content increased to 1.0%, which was about 0.07 W/(m K) higher than the initial 0.47 W/(m K) for pure PDMAA hydrogel. It can be seen from Table 3 that the thermal conductivity persistently increased along with the increment of GR content without any slow-down trend, which means that much higher thermal conductivity than 0.54 W/(m K) could be achieved in the case of more GR was added.

Moreover, information about the electrical conductivity of PDMAA/GR nanocomposite hydrogels is summarized and depicted in Table 4. Considering the fact that electrical conductivity may be affected by the water content in hydrogel networks, various hydrogels synthesized with different water contents (70% and 80.6%) were taken to perform conducting test. With water content of 80.6%, this series of hydrogels exhibited higher electrical conductivity than the other group. The conductivity increased from initial 0.885×10^{-3} S/m to 1.29×10^{-3} S/m for 1.0% GR, achieving a conductivity growth of 46%. The electrical conductivities under water content of 70% were overall lower than the previous group, increasing from initial 0.366×10^{-3} S/m to 1.45×10^{-3} S/m or 1.0% graphene mass ratio. However, GR will be diluted by increased water content and it was difficult to generate perfect conductive circuit created by GR nanofiller. Based on this, the electrical conductivity of $PBG_{1.0}H$ with 70% water content was higher than that with 80.6% water content. It should be noted that the mass ratio of graphene in the whole PDMAA/GR/water system was only 0.19% when 1.0% GR content against DMAA monomers was used.

Table 4 Electrical properties of PDMAA/graphene nanocomposite hydrogels

Sample	Conductivity ($\times 10^{-3}$)/S/m	
	70% water	80.6% water
PBH	0.366	0.885
$PBG_{0.1}H$	0.439	1.04
$PBG_{0.4}H$	0.494	1.09
$PBG_{0.7}H$	0.683	1.16
$PBG_{1.0}H$	1.45	1.29

Conclusions

In summary, strong and conductive polymer/pristine GR nanocomposite hydrogel was directly synthesized by applying DMAA as reactive monomers and dispersion solvent, while pristine GR as conductive nanofillers. Such fabrication route was feasible owing to the strong interaction between DMAA and GR, which was deeply investigated through UV–Vis, ^{1}H NMR and rheological measurement in our work. These results are helpful for us to understand the interaction mechanism between amide monomers and graphene. Conclusions were made that the addition of GR into PDMAA hydrogel improved the dimensional homogeneity of pore structure, the stretching and compression properties and the swelling ratio, as well as thermal and electrical conductivity. This study gives inspiration for researches to handily synthesize conductive polymeric hydrogel without unpleasant intermediate procedures.

Acknowledgements

This work was financially supported by National Natural Science Foundation of China (Nos. 51803105, 51703113 and 51703111), Shandong Provincial Natural Science Foundation (Nos. ZR2019QEM002, ZR2017BEM039 and ZR2017BEM011) and China Postdoctoral Science Foundation (2018M642717 and 2018M630763).

References

[1] Pan C, Liu L, Gai G (2017) Recent progress of graphene-containing polymer hydrogels: preparations, properties, and applications. Macromol Mater Eng 302:184–198

[2] Laftah WA, Hashim S, Ibrahim AN (2011) Polymer hydrogels: a review. Polym Plast Technol Eng 50:1475–1486

[3] Homaeigohar S, Tsai TY, Young TH, Yang HJ, Ji YR (2019) An electroactive alginate hydrogel nanocomposite reinforced by functionalized graphite nanofilaments for neural tissue engineering. Carbohydr Polym 224:1–13

[4] Gaharwar AK, Peppas NA, Khademhosseini A (2014) Nanocomposite hydrogels for biomedical applications. Biotechnol Bioeng 111:441–453

[5] Haraguchi K, Uyama K, Tanimoto H (2011) Self-healing in nanocomposite hydrogels. Macromol Rapid Commun 32:1253–1258

[6] Kabiri K, Omidian H, Zohuriaan-Mehr MJ, Doroudiani S (2011) Superabsorbent hydrogel composites and nanocomposites: a review. Polym Compos 32:277–289

[7] Sabzi M, Samadi N, Abbasi F, Mahdavinia GR, Babaahmadi M (2017) Bioinspired fully physically cross-linked double network hydrogels with a robust, tough and self-healing structure. Mater Sci Eng C Mater Biol Appl 74:374–381

[8] Shi Y, Peng L, Yu G (2015) Nanostructured conducting polymer hydrogels for energy storage applications. Nanoscale 7:12796–12806

[9] Haraguchi K (2007) Nanocomposite hydrogels. Curr Opin Solid St Mater Sci 11:47–54

[10] Wang T, Huang J, Yang Y, Zhang E, Sun W, Tong Z (2015) Bioinspired smart actuator based on graphene oxide-polymer hybrid hydrogels. ACS Appl Mater Interfaces 7:23423–23430

[11] Hu K, Kulkarni DD, Choi I, Tsukruk VV (2014) Graphene-polymer nanocomposites for structural and functional applications. Prog Polym Sci 39:1934–1972

[12] Chen F, An W, Li Y, Liang Y, Cui W (2018) Fabricating 3D porous PANI/TiO_2–graphene hydrogel for the enhanced UV-light photocatalytic degradation of BPA. Appl Surf Sci 427:123–132

[13] Haraguchi K, Farnworth R, Ohbayashi A, Takehisa T (2003) Compositional effects on mechanical properties of nanocomposite hydrogels composed of poly(*N*,*N*-dimethylacrylamide) and clay. Macromolecules 36:5732–5741

[14] Wu D, Yi M, Duan H, Xu J, Wang Q (2016) Tough TiO_2–rGO–PDMAA nanocomposite hydrogel via one-pot UV polymerization and reduction for photodegradation of methylene blue. Carbon 108:394–403

[15] Xu D, Bhatnagar D, Gersappe D, Sokolov JC, Rafailovich MH, Lombardi J (2015) Rheology of poly(*N*-isopropylacrylamide)–clay nanocomposite hydrogels. Macromolecules 48:840–846

[16] Mourycova J, Datta KKR, Prochazkova A, Plotena M, Enev V, Smilek J, Masilko J, Pekar M (2018) Facile synthesis and rheological characterization of nanocomposite hyaluronan-organoclay hydrogels. Int J Biol Macromol 111:680–684

[17] Ramon-Azcon J, Ahadian S, Estili M, Liang X, Ostrovidov S, Kaji H, Shiku H, Ramalingam M, Nakajima K, Sakka Y, Khademhosseini A, Matsue T (2013) Dielectrophoretically aligned carbon nanotubes to control electrical and mechanical properties of hydrogels to fabricate contractile muscle myofibers. Adv Mater 25:4028–4034

[18] Cong HP, Qiu JH, Yu SH (2015) Thermoresponsive poly(*N*-isopropylacrylamide)/ graphene/Au nanocomposite hydrogel for water treatment by a laser-assisted approach. Small 11:1165–1170

[19] Alam A, Zhang Y, Kuan HC, Lee SH, Ma J (2018) Polymer composite hydrogels containing carbon nanomaterials-morphology and mechanical and functional performance. Prog Polym Sci 77:1–18

[20] Du G, Nie L, Gao G, Sun Y, Hou R, Zhang H, Chen T, Fu J (2015) Tough and biocompatible hydrogels based on in situ interpenetrating networks of dithiol-connected graphene oxide and poly(vinyl alcohol). ACS Appl Mater Interfaces 7:3003–3008

[21] Alam A, Kuan HC, Zhao Z, Xu J, Ma J (2017) Novel polyacrylamide hydrogels by highly conductive, water-processable graphene. Compos Part A Appl Sci Manuf 93:1–9

[22] Huang W, Shen J, Li N, Ye M (2015) Study on a new polymer/graphene oxide/clay double network hydrogel with improved response rate and mechanical properties. Polym Eng Sci 55:1361–1366

[23] Lo CW, Zhu D, Jiang H (2011) An infrared-light responsive graphene-oxide incorporated poly(*N*-isopropylacrylamide) hydrogel nanocomposite. Soft Matter 7:5604–5609

[24] Jo H, Sim M, Kim S, Yang S, Yoo Y, Park JH, Yoon TH, Kim MG, Lee JY (2017) Electrically conductive graphene/polyacrylamide hydrogels produced by mild chemical reduction for enhanced myoblast growth and differentiation. Acta Biomater 48:100–109

[25] Liu W, Zhou R, Zhou D, Ding G, Soah JM, Yue CY, Lu X (2015) Lignin-assisted direct exfoliation of graphite to graphene in aqueous media and its application in polymer composites. Carbon 83:188–197

[26] Hou C, Duan Y, Zhang Q, Wang H, Li Y (2012) Bio-applicable and electroactive near-infrared laser-triggered self-healing hydrogels based on graphene networks. J Mater Chem 22:14991–14996

[27] Tavsanli B, Can V, Okay O (2015) Mechanically strong triple network hydrogels based on hyaluronan and poly(*N*,*N*-dimethylacrylamide). Soft Matter 11:8517–8524

[28] Moghanjoughi AA, Khoshnevis D, Zarrabi A (2016) A concise review on smart polymers for controlled drug release. Drug Deliv Transl Res 6:333–340

[29] Zhao P, Xu J, Zhang Y, Zhu W, Cui Y (2018) Polymerizable-group capped ZnS nanoparticle for high refractive index inorganic-organic hydrogel contact lens. Mater Sci Eng C Mater Biol Appl 90:485–493

[30] Algi MP, Okay O (2014) Highly stretchable self-healing poly(*N*,*N*-dimethylacrylamide) hydrogels. Eur Polym J 59:113–121

[31] Pandey VS, Verma SK, Yadav M, Behari K (2014) Guar gum-g-*N*,*N*′-dimethylacrylamide: synthesis, characterization and applications. Carbohydr Polym 99:284–290

[32] Chen HY, Hayashi T, Koenig M, Lai JJ (2019) Polymer surface chemistry: biomolecular engineering and biointerfaces. Front Chem 7:271–274

[33] Homaeigohar S, Dai T, Elbahri M (2013) Biofunctionalized nanofibrous membranes as super separators of protein and enzyme from water. J Colloid Interface Sci 406:86–93

[34] Zhao F, Zhang G, Zhao S, Cui J, Gao A, Yan Y (2018) Fabrication of pristine graphene-based conductive polystyrene composites towards high performance and lightweight. Compos Sci Technol 159:232–239

[35] Bekiari V, Lianos P (2006) Photophysical behavior of terpyridine-lanthanide ion complexes incorporated in a poly(*N*,*N*-dimethylacrylamide) hydrogel. Langmuir 22:8602–8606

[36] Guillaumont L, Bokias G, Iliopoulos I (2000) Hydrophobically modified poly(*N*,*N*-dimethylacryl-amide): Synthesis, aqueous solution behaviour, and rheological properties in aqueous mixtures with hydrophobically modified poly(-sodium acrylate). Macromol Chem Phys 20:251–260

[37] Song G, Zhang L, He C, Fang DC, Whitten PG, Wang H (2013) Facile fabrication of tough hydrogels physically cross-linked by strong cooperative hydrogen bonding. Macromolecules 46:7423–7435

[38] Pontefisso A, Mishnaevsky L (2016) Nanomorphology of graphene and CNT reinforced polymer and its effect on damage: micromechanical numerical study. Compos Part B Eng 96:338–349